PAPER

Fermi-liquid behavior of binary intermetallic compounds Y_3M (M = Co, Ni, Rh, Pd, Ir, Pt)

Materials Research Express

PAPER

Fermi-liquid behavior of binary intermetallic compounds Y_3M (M = Co, Ni, Rh, Pd, Ir, Pt)

RECEIVED
14 December 2016

REVISED
7 April 2017

ACCEPTED FOR PUBLICATION
21 April 2017

PUBLISHED
1 June 2017

Judyta Strychalska-Nowak[1], Bartłomiej Wiendlocha[2], Katarzyna Hołowacz[1], Paula Reczek[1], Mateusz Podgórski[1], Michał J Winiarski[1] and Tomasz Klimczuk[1]

[1] Faculty of Applied Physics and Mathematics, Gdansk University of Technology, Narutowicza 11/12, 80-233 Gdansk, Poland
[2] Faculty of Physics and Applied Computer Science, AGH University of Science and Technology, Aleja Mickiewicza 30, 30-059 Krakow, Poland

E-mail: jstrychalska@mif.pg.gda.pl **and** tomasz.klimczuk@pg.gda.pl

Keywords: intermetallic compounds, electrical resistivity, heat capacity, x-ray diffraction, Fermi liquid, electronic structure calculations

Abstract

A series of polycrystalline samples of Y_3M (M = Co, Ni, Rh, Pd, Ir, Pt), intermetallic binary compounds were synthesized by the arc-melting method. Powder x-ray diffraction (pXRD) confirmed the orthorhombic cementite-type crystal structure and allowed for the estimation of the lattice parameters. Physical properties were investigated by means of electrical resistivity and heat capacity measurements between 1.9 K and 300 K. All tested compounds show metallic-like behaviour with RRR values ranging from 1.3 to 8.3, and power-law $\rho \propto T^n$ temperature dependence of resistivity was observed, with $1.6 \leqslant n \leqslant 2.2$. No superconductivity was detected above 1.9 K. The Debye temperature, estimated from the low temperature heat capacity fit, ranged from 180 K (Y_3Pt) to 222 K (Y_3Co). The highest value of the Sommerfeld coefficient γ was found for Y_3Pd (19.5 mJ mol^{-1} K^{-2}). The pXRD pattern of Y_3Rh indicated the presence of Y_5Rh_2, a previously unreported Pd_5B_2-type phase, whose unit cell parameters were refined using the LeBail method. Density functional theory calculations were performed and theoretical results revealed strong enhancement of the measured electronic specific heat, which was 30%–100% larger than computed. Quadratic temperature dependence of resistivity and enhanced electronic specific heat indicated a Fermi-liquid behavior of electrons in these materials.

1. Introduction

Among binary intermetallic compounds, the Fe_3C-type (cementite) crystal structure is one of the most common [1]. The prototypic compound Fe_3C crystallizes in a low symmetry, orthorhombic (*Pnma*) structure with a unit cell containing 12 iron and 4 carbon atoms (4 formula units) and its properties have been studied for decades due to its importance in metallurgy.

Binary compounds with the formula R_3M, where R is a rare-earth metal and M is a transition metal from group 9 or 10, exhibit various interesting physical properties. In the unit cell, the M atom is located inside a trigonal prism formed by the surrounding R atoms. The crystal structure of Y_3M compounds is presented in figure 1.

In such a crystal structure a typical distance between M atoms is large and exceeds 4.3 Å, whereas the distance between R metal atoms can be 20% shorter, i.e. 3.5 Å (Y_3Co). The d band of the transition metal is filled by electrons from the rare-earth atoms and hence no magnetic moments on the M atoms are observed.

In a large R_3M family, R_3Co and R_3Ni have attracted much attention. Most of the R_3Co compounds reveal a complicated magnetic structure, with the magnetic moment carried by a rare-earth metal (R). The highest Néel temperature (T_N = 131 K) with a field-induced magnetic transition from an antiferromagnetic (AFM) to a ferromagnetic (FM) state, was reported for Gd_3Co [3, 4]. The absence of a magnetic moment for Co has been confirmed for R_3Co compounds with non-magnetic R = Y and La. Interestingly, La_3Co reveals superconductivity with T_c = 4.5 K [5, 6] whereas Y_3Co exhibits a charge density wave (CDW) instability [5]. Geballe *et al* [5] reported superconductivity for Y_3Rh (T_c = 0.65 K) and traces of superconductivity for Y_3Co with $T_{c\,onset}$ at 0.34 K. To the best of our knowledge superconductivity for Y_3Co was neither confirmed nor studied.

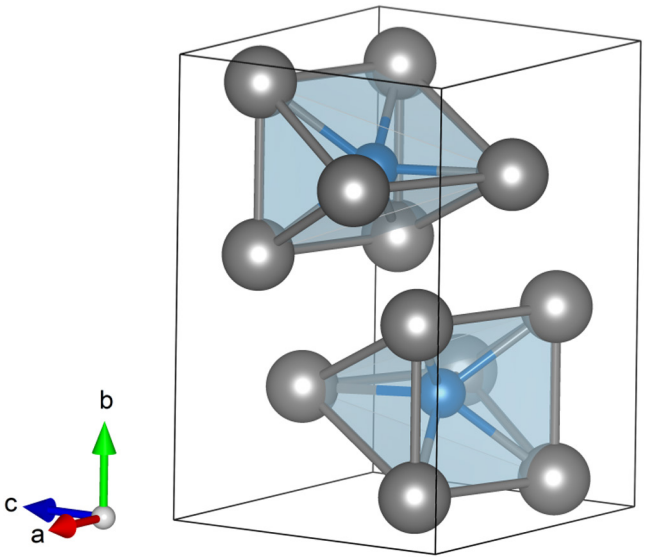

Figure 1. Crystal structure of cementite-type Y_3M intermetallic compound. Transition metal atoms (blue) at 4*c* site are surrounded by yttrium atoms (grey) from 8*d* and 4*c* positions, forming trigonal prisms [2].

Weak spin fluctuations have been observed in Y_3Ni that influence its physical properties [6]. In particular, the low temperature region of the electrical resistivity is proportional to T^2, characteristic for a Fermi liquid, and has a tendency for saturation at high temperatures. No superconductivity above 20 mK was found in Y_3Ni [7]. Physical properties of the Y_3M compounds where M = Rh, Pd have not been studied extensively [8, 9], and only the crystal structure was reported for M = Ir, Pt [8, 10].

This study is a report of the synthesis and physical properties of the Y_3M family, where M = Co, Rh, Ir,Ni, Pd, and Pt. The results presented here allow a direct comparison of the influence of the M metal on the physical properties in this interesting Y_3M family.

2. Experimental

Polycrystalline samples of Y_3M were synthesized by arc-melting stoichiometric amounts of yttrium, and the transition metal M = Co, Ni, Rh, Pd, Ir and Pt with purity 99.95% or higher. Melting took place in a water-cooled copper hearth, under a high-purity argon atmosphere. A zirconium button was used as a nitrogen and oxygen getter. All samples were remelted four times and flipped over each time to ensure homogeneity of the material. The mass loss of the melted products was below 0.5%. The prepared samples were wrapped in tantalum foil, placed in sealed quartz tubes and annealed for 3 weeks. Temperatures of annealing were 900 °C for Y_3Ir, Y_3Pt, Y_3Pd and 850 °C for Y_3Co, Y_3Ni, Y_3Rh.

Powder x-ray diffraction (pXRD) analysis on ground material was carried out on a PANalytical X'Pert Pro with a Cu-Kα radiation source. The LeBail refinements of the structural model against the x-ray data were performed using FullProf software [11]. The morphology of the samples was characterized using scanning electron microscopy (SEM) FEI Quanta 250 FEG under high vacuum with an accelerating voltage of 30 kV. To recognize the elements and their distribution in studied samples the energy-dispersive x-ray spectroscopy (EDS) was performed using an EDAX Apollo X silicon drift detector. The EDS spectra were processed by means of a standardless analysis method using the EDAX TEAM software.

The physical properties were examined through measurements of heat capacity, magnetic susceptibility and electrical resistivity using a quantum design physical property measurement system (PPMS).

3. Results and discussion

The powder x-ray diffraction profiles of all studied samples are presented in figure 2.

Since the cementite crystal structure (*Pnma*, s.g. # 62) has low symmetry, and relatively large lattice parameters, more than 70 Bragg peaks with low intensities are observed for 2Θ in the range 15°–60°. The LeBail refinement confirms the Fe_3C-type structure of examined compounds with estimated lattice parameters (table 1) are in good agreement with literature [9, 10, 12–14]. The lattice parameters, and the unit cell volume, increase with the column of the M element (Co–Rh–Ir, and Ni–Pd–Pt). It is worth noting that changing the M atom from group 9

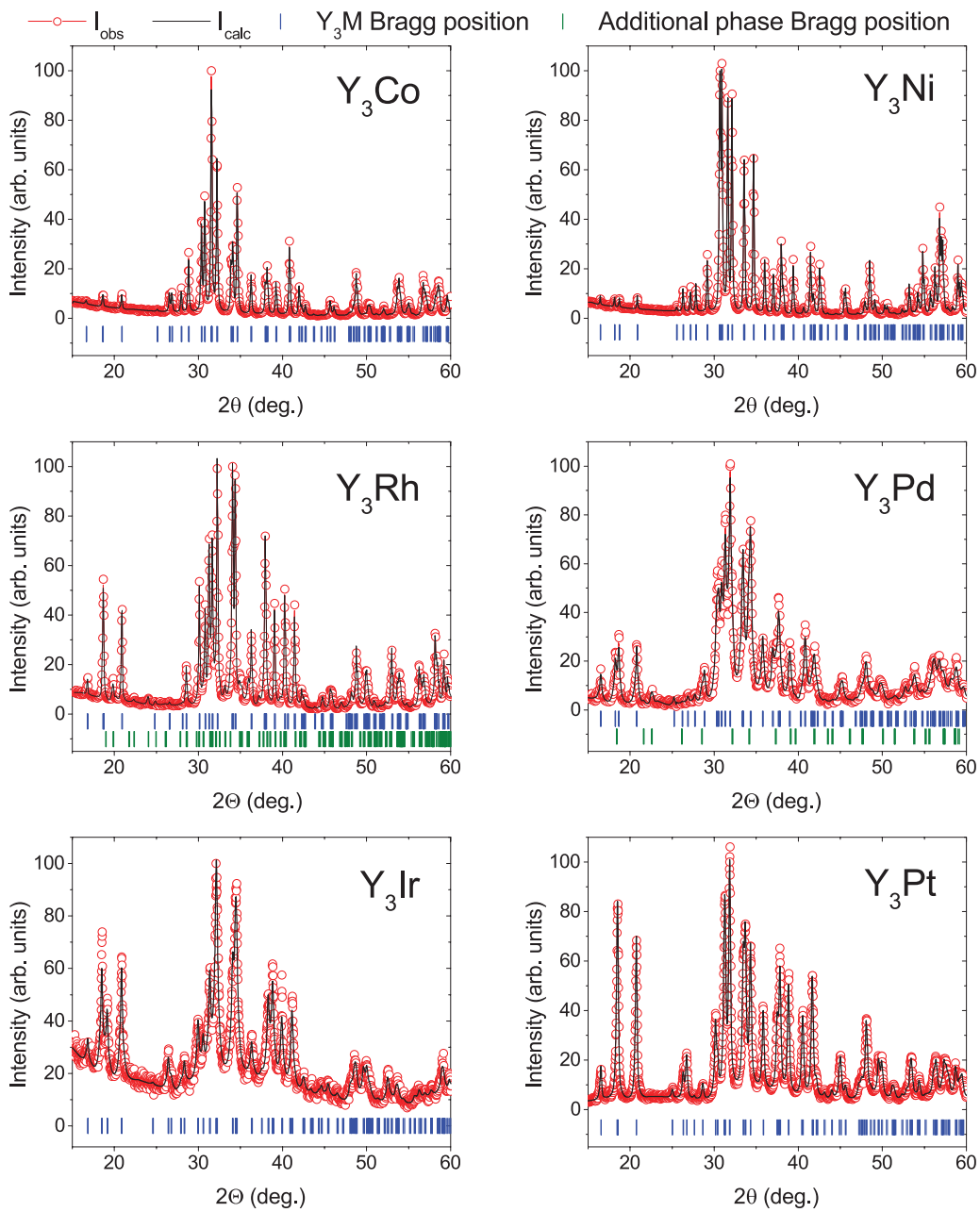

Figure 2. Le Bail refinements of the powder x-ray diffraction data for examined Y_3M samples. The open, red circles represent the observed x-ray patterns, the solid, black lines represent the fitted pattern, and the vertical bars represent the peak positions of the Fe_3C-type phase (blue) and impurity (green).

Table 1. Lattice constants, unit cell volume, and parameters of the LeBail refinements for Y_3M. In the case of Y_3Rh and Y_3Pd the model included the second phase (Y_5Rh_2 and $Y_{4.86}Pd_2$, respectively).

	Y_3Co	Y_3Ni	Y_3Rh	Y_3Pd	Y_3Ir	Y_3Pt
a (Å)	7.035(1)	6.908(1)	7.177(1)	7.061(1)	7.247(1)	7.101(4)
b (Å)	9.426(1)	9.642(1)	9.466(1)	9.729(1)	9.276(3)	9.584(7)
c (Å)	6.336(1)	6.355(1)	6.345(1)	6.443(1)	6.404(3)	6.454(6)
V (Å^3)	420(3)	423(5)	431(6)	442(3)	430(2)	439(4)
R_p	9.8	8.06	7.3	13.7	19.4	9.3
R_{wp}	11.7	9.35	9.1	16.8	20.6	11.5
R_{exp}	7.0	5.7	5.5	15.0	17.9	9.3
χ^2	2.83	2.74	2.71	1.26	1.51	1.54

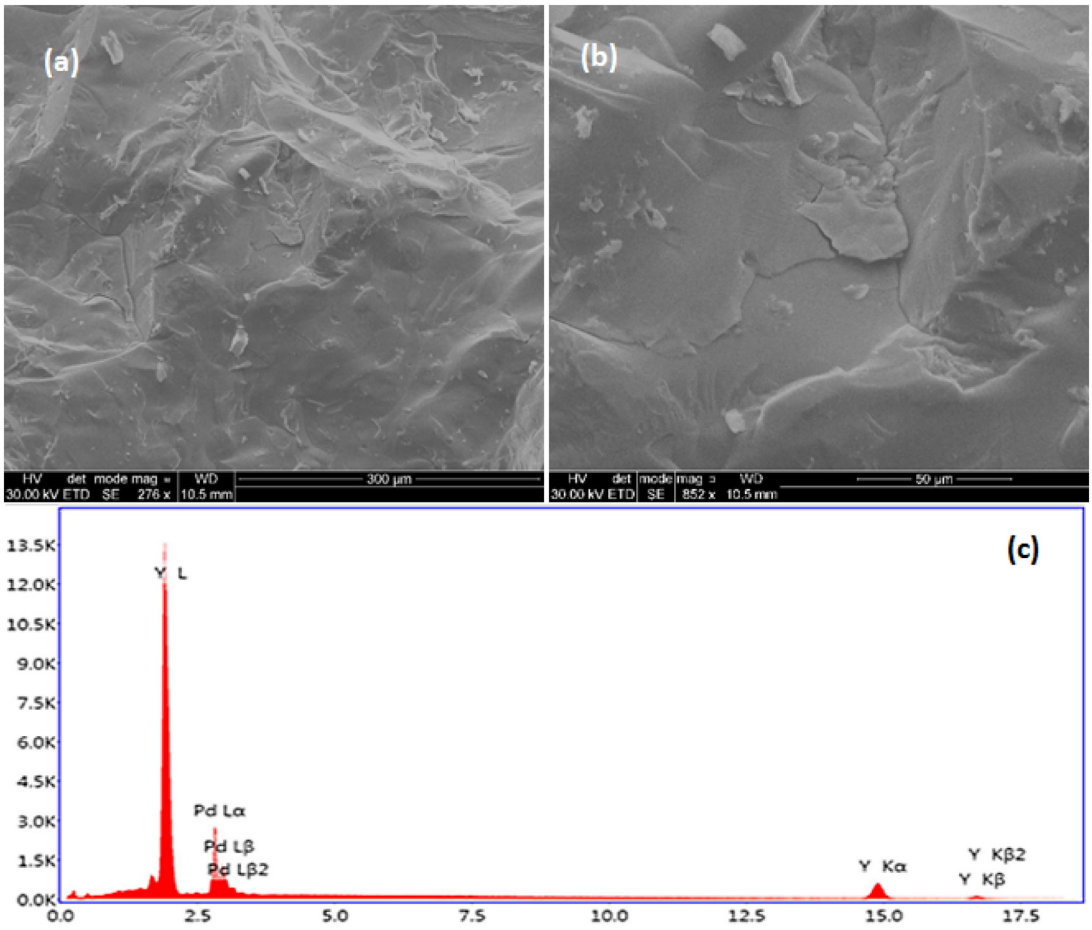

Figure 3. (a) and (b) SEM images and (c) EDS spectrum of the Y_3Pd sample.

(Co, Rh, Ir) to group 10 (Ni, Pd, Pt) causes a decrease of a and an increase in both the b and c lattice parameters. Overall, the unit cell volume increases.

The pXRD patterns for Y_3Pd, Y_3Pt and Y_3Rh indicate a small amount of $Y_{4.86}Pd_2$ [15], the unknown phase and Y_5Rh_2, respectively. The latter phase is a previously unreported structural analogue of the Pd_5B_2-type Y_5Ir_2 compound [16]. Refinement of the lattice constant for $Y_{4.86}Pd_2$ yielded the lattice constant $a = 13.637$ Å, which is in very good agreement with the reported value (13.625 Å [15]).

The new compound Y_5Rh_2 crystallizes in a monoclinic structure (space group $C2/c$, no. 15, Pearson symbol $mS28$). A LeBail fit to the pXRD pattern yields lattice constants $a = 16.037(4)$ Å, $b = 6.407(1)$ Å, $c = 7.192(2)$ Å, and $\beta = 97.09(2)°$. The obtained lattice parameters are similar to those reported for isostructural Y_5Ir_2 [16] and slightly smaller than for Eu_5Rh_2 [17].

The morphology of all samples was studied using SEM microscopy. Sample images of the fracture surface of Y_3Pd are shown in figures 3(a) and (b).

The SEM pictures made for all Y_3M samples reveal irregular cracks, fractures and separate particles. The energy dispersive spectroscopy (EDS) confirms nominal chemical composition of the samples. The illustrative EDS spectrum for Y_3Pd is shown in figure 3(c).

The temperature dependence of the normalized resistivity $\rho(T)/\rho(300\,K)$ of Y_3M in the temperature range 1.9 K–300 K is shown in figures 4(a) and (b).

All specimens show a metallic-like character ($d\rho/dT > 0$) with no superconducting transition observed above 1.9 K. A characteristic hump at around 160 K is observed for the Y_3Co compound and was first reported by Talik *et al* [12]. This feature is caused by the charge density instability and was studied in detail by Podlesnyak *et al* [18]. An almost linear shape of $\rho(T)$ above 40 K is seen for the Y_3Rh sample, which shows the lowest value of residual resistivity $\rho(2\,K)$.

The residual resistivity ratio, $RRR = \rho(300\,K)/\rho(2\,K)$, is between 1.3 ($Y_3Ir$) and 8.3 ($Y_3Pd$). It is worth noting that the RRR value for intermetallic compounds in the polycrystalline form can be as high as 26, reported for weak ferromagnetic superconductor Y_9Co_7 [19], and between 1 and 2 for highly disordered, yet superconducting, Heusler-type compounds [20].

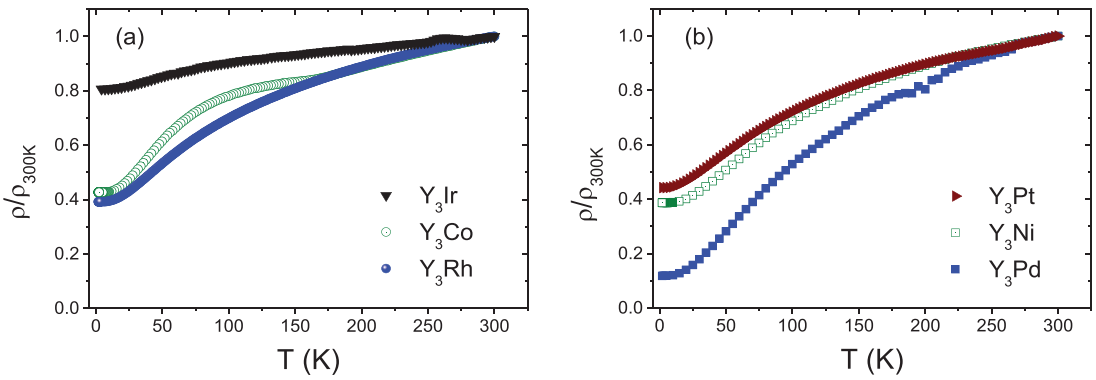

Figure 4. Normalized electrical resistivity ($\rho/\rho_{300\,K}$) for (a) Y_3Co, Y_3Rh, Y_3Ir and (b) Y_3Ni, Y_3Pd, Y_3Pt, respectively.

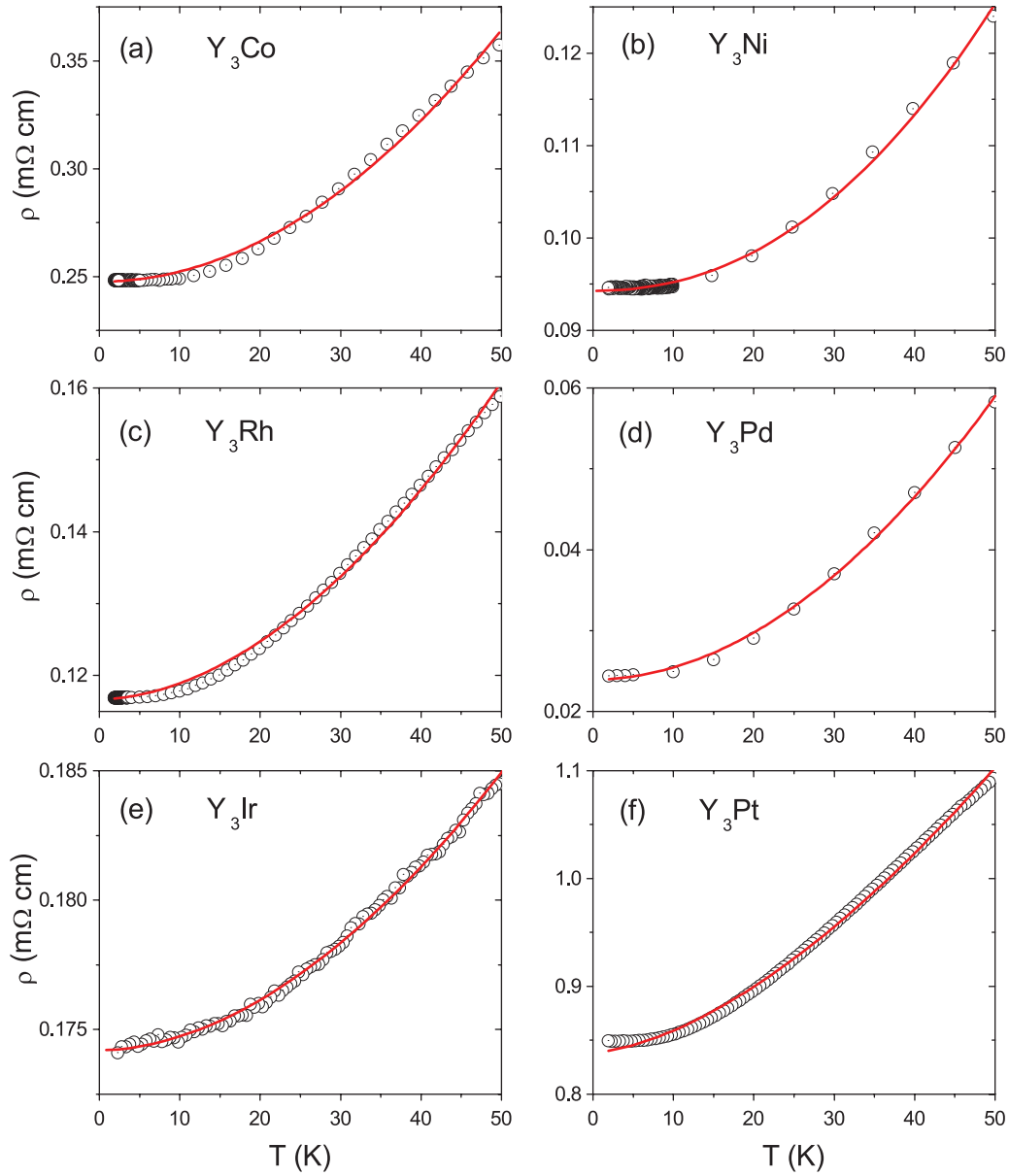

Figure 5. Low temperature resistivity data (open circles) for Y_3M compounds ((a) Y_3Co, (b) Y_3Ni, (c) Y_3Rh, (d) Y_3Pd, (e)Y_3Ir, (f) Y_3Pt) with $\rho(T) = \rho_0 + AT^n$ fits (solid lines).

Temperature dependence of electrical resistivity suggest the presence of weak electron–electron interactions of the Fermi liquid type. Moreover, Gratz *et al* discussed possible spin fluctuations and their influence on the physical properties of Y_3Ni [21]. In particular, they showed that $\rho(T)$ for Y_3Ni has a tendency for saturation at high temperature and shows $\rho(T) = \rho_0 + AT^2$ behavior in the low temperature region, as it is also seen in our studies.

Table 2. Physical properties parameters for Y_3M .

	Y_3Co	Y_3Ni	Y_3Rh	Y_3Pd	Y_3Ir	Y_3Pt
ρ(2 K) (mΩ cm)	0.25	0.095	0.12	0.025	0.17	0.85
ρ(300 K) (mΩ cm)	0.58	0.244	0.30	0.207	0.22	1.92
RRR	2.3	2.6	2.5	8.3	1.3	2.3
ρ_0 (mΩ cm)	0.25	0.094	0.12	0.024	0.17	0.84
A (10^{-3} $\mu\Omega$ cm K^{-n})	47.4	6.0	31	16.6	7.4	500
n	2.00(3)	2.19(3)	1.86(2)	1.96(6)	1.86(2)	1.60(2)
A ($n = 2$) (10^{-3} $\mu\Omega$ cm K^{-2})	48.3	4.5	18.2	13.6	12.2	—
γ (mJ mol^{-1} K^{-2})	16.70(9)	15.5(2)	18.6(3)	19.5(2)	14.0(2)	16.8(3)
β (mJ mol^{-1} K^{-4})	0.708(9)	0.73(2)	1.31(2)	1.06(2)	1.01(3)	1.32(2)
Θ_D (K)	222(9)	219(2)	186(2)	194(1)	197(2)	180(1)
Θ_E (K)	—	285(8)	337(11)	325(6)	211(5)	199(4)
K	1	0.72	0.79	0.91	0.92	0.82
$A/\gamma^2(n)$ Ω m (J mol^{-1} $K^{-1})^{-2}$	17×10^{-7}	2.5×10^{-7}	9×10^{-7}	4.4×10^{-7}	3.8×10^{-7}	—
A/γ^2 ($n = 2$ fixed) Ω m (J mol^{-1} $K^{-1})^{-2}$	17×10^{-7}	1.9×10^{-7}	5.4×10^{-7}	3.6×10^{-7}	6.3×10^{-7}	—

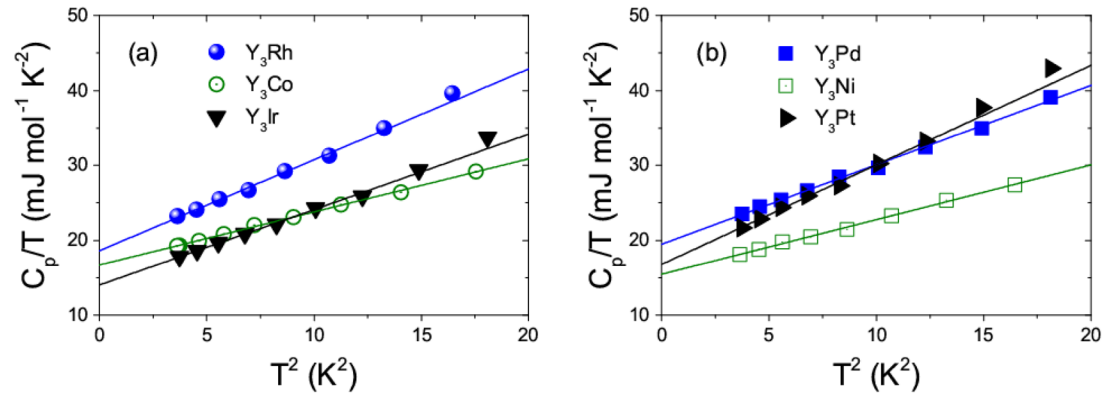

Figure 6. Low-temperature C_p/T versus T^2 for (a) Y_3Co, Y_3Rh, Y_3Ir and (b) Y_3Ni, Y_3Pd, Y_3Pt. Solid lines are the fit of the heat capacity data by $C_p(T)/T = \gamma + \beta T^2$.

In figure 5 we present temperature dependence of $\rho(T)$ and a solid line through the resistivity data is a fit by the formula $\rho(T) = \rho_0 + AT^n$. The fitting parameters are gathered in table 2, and almost quadratic ($n \simeq 2$) low temperature resistivity behavior is observed for all studied compounds, except Y_3Pt, for which the estimated exponent n is slightly lower, $n = 1.6$. The value of n for Y_3Pt is close to 5/3, observed, in addition to $n = 2$, in various spin fluctuating systems, e.g. in magnetic superconductor Y_4Co_3 [22].

Quadratic temperature dependence of resistivity ($n = 2$) is characteristic for a system of interacting electrons, as predicted by the Landau theory of the Fermi liquid [23], thus a second set of fitted A parameter, with $n = 2$ fixed, is presented in table 2. For Y_3Ni the prefactor $A = 4.5 \cdot 10^{-3}$ $\mu\Omega$ cm K^{-2} is lower than estimated by Gratz *et al* [7] $A = 10.9 \cdot 10^{-3}$ $\mu\Omega$ cm K^{-2}. The reported A values for the relevant binaries with lanthanum are: $16 \cdot 10^{-3}$ $\mu\Omega$ cm K^{-2} and $28 \cdot 10^{-3}$ $\mu\Omega$ cm K^{-2} for La_3Ni and La_3Co, respectively [6].

Low temperature specific heat (C_p/T) versus T^2 is shown in figure 6.

As it can be seen, C_p/T is linearly related to T^2 and the Debye temperature (Θ_D) and the Sommerfeld coefficient (γ) can be estimated from:

$$C_p/T = \gamma + \beta T^2. \quad (1)$$

In this equation the β parameter is related to the Debye temperature through $\Theta_D = \left(\frac{12\pi^4}{5\beta} nR\right)^{1/3}$ where n is the number of atoms per formula unit ($n = 4$) and R is the gas constant ($R = 8.314$ J mol^{-1} K^{-1}). For a Fermi liquid, the linear coefficient γ is additionally renormalized due to the electron–electron interactions: $\gamma = \gamma_0 \frac{m^*}{m}$, where γ_0 is the non-interacting value, and effective mass m^* includes all the effects of electronic interactions. The fits to equation (1) are shown as the solid straight lines through the heat capacity (C_p/T) data points in figures 6(a) and (b). The fit parameters obtained for Y_3M are gathered in table 2. The highest estimated Θ_D is observed for compounds containing light transition metals: Y_3Co ($\Theta_D = 222$ K) and Y_3Ni ($\Theta_D = 219$ K). These temperatures are in very good

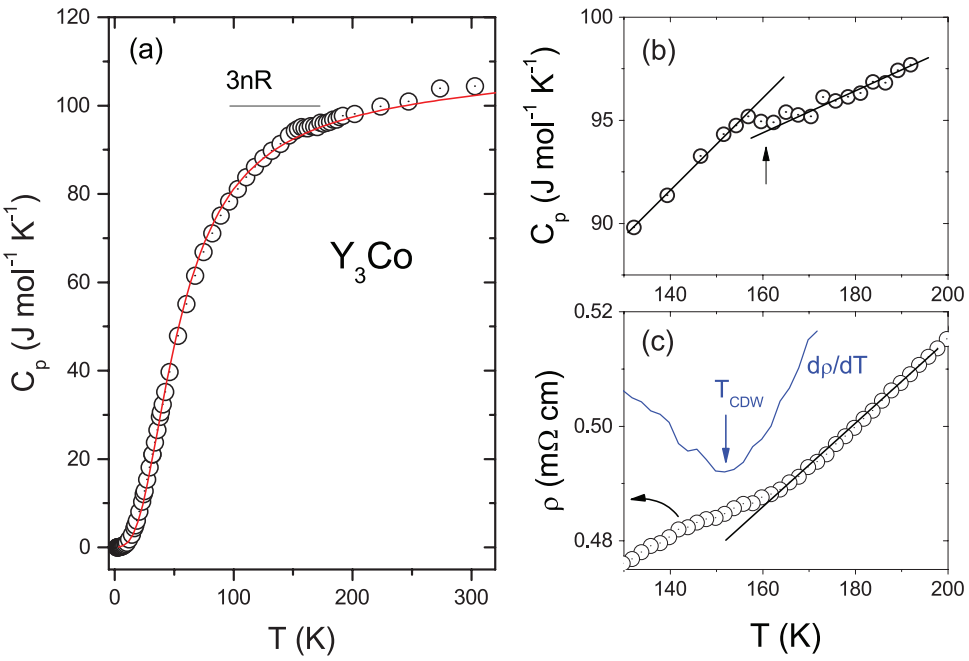

Figure 7. (a) Temperature dependence of heat capacity for Y_3Co. The red line is the fitted sum of the electronic specific heat (γT) and phonon specific heat from the Debye model; (b) the heat capacity in vicinity of the T_{CDW}; (c) open circles are resistivity data points, and a blue, solid line is dρ/dT between 135 K and 200 K.

agreement with $\Theta_D = 223$ K [4] and 243 K [24] reported for Y_3Co and Y_3Ni, respectively. As expected, the Debye temperature is lower for Y_3M compounds with the M metal from the fifth and sixth periods [4, 24, 25].

The highest Sommerfeld coefficient (γ), is revealed for Y_3Pd (19.5 mJ mol^{-1} K^{-2}).

Having values of γ and A, we can calculate the Kadowaki–Woods ratio (A/γ^2). Estimated values of A/γ^2 (for $n = 2$ resistivity fit) ranges from $A/\gamma^2 = 17 \cdot 10^{-7}\,\Omega$ m (J mol^{-1} K^{-1})$^{-2}$ and $1.9 \cdot 10^{-7}\,\Omega$ m (J mol^{-1} K^{-1})$^{-2}$ for Y_3Co and Y_3Ni, respectively. The first is four times larger than $A/\gamma^2 = 4.6 \cdot 10^{-7}\,\Omega$ m (J mol^{-1} K^{-1})$^{-2}$ reported for the La_3Co superconductor [26], and the second is close to $2.8 \cdot 10^{-7}\,\Omega$ m (J mol^{-1} K^{-1})$^{-2}$ reported for La_3Ni [27]. The obtained values of A/γ^2 are close to the 'universal' $10^{-7}\,\Omega$ m (J mol^{-1} K^{-1})$^{-2}$ observed in heavy-fermion compounds [12]. Since the low temperature resistivity for Y_3Pt deviates most from a quadratic behavior, the Kadowaki–Woods ratio for this compound is not provided.

The specific heat data $C_p(T)$ between 1.9 K and 300 K for Y_3Co is presented in figure 7(a).

At high temperature, C_p saturates slightly above the expected Dulong–Petit value $3nR \approx 100$ J mol^{-1} K^{-1}. The experimental data were fitted in the whole temperature range by using the following formula:

$$C_p = \gamma T + C_{\mathrm{Debye}}(T). \tag{2}$$

The first term (γT) is an electronic contribution to the specific heat, which is discussed in the next section, and the second is a phonon contribution to the specific heat given by the Debye (C_{Debye}) model:

$$C_{\mathrm{Debye}}(T) = 9nR\left(\frac{T}{\Theta_D}\right)^3 \int \frac{x^4 \exp(x)}{[\exp(x) - 1]^2} \mathrm{d}x. \tag{3}$$

In figure 7(a), a red solid curve through the data is a fit to expression (2). The Debye temperature estimated from the fit $\Theta_D = 220$ K is in good agreement with the Debye value obtained from the low temperature fit by using formula (1).

The neutron scattering techniques were used to study Y_3Co, and it was concluded that the CDW formation around 160 K results in an unusually strong lattice distortion [18]. A heat capacity anomaly shown in figure 7(b) appears at 160 K in perfect agreement with the temperature of the C_p anomaly reported in [18]. Electrical resistivity (open circles) and the temperature derivative of electrical resistivity (dρ/dT) in the vicinity of the charge density wave formation temperature (T_{CDW}) are presented in figure 7(c). The T_{CDW} temperature estimated as the minimum of dρ/dT [18] is slightly lower with a value of 152 K.

Figure 8 presents the temperature dependence of the specific heat (C_p) for Y_3Rh (a) and Y_3Ir (b) compounds.

Using the derived low temperature Θ_D—the calculated Debye phonon contribution (C_{Debye}) to the specific heat is not large enough to reach experimental C_p data above 100 K and 75 K for Y_3Rh and Y_3Ir, respectively. The difference between C_{Debye} and C_p indicates that the high energy optical modes must be present. Therefore, the C_p data points were fitted in the whole temperature range by using the following formula:

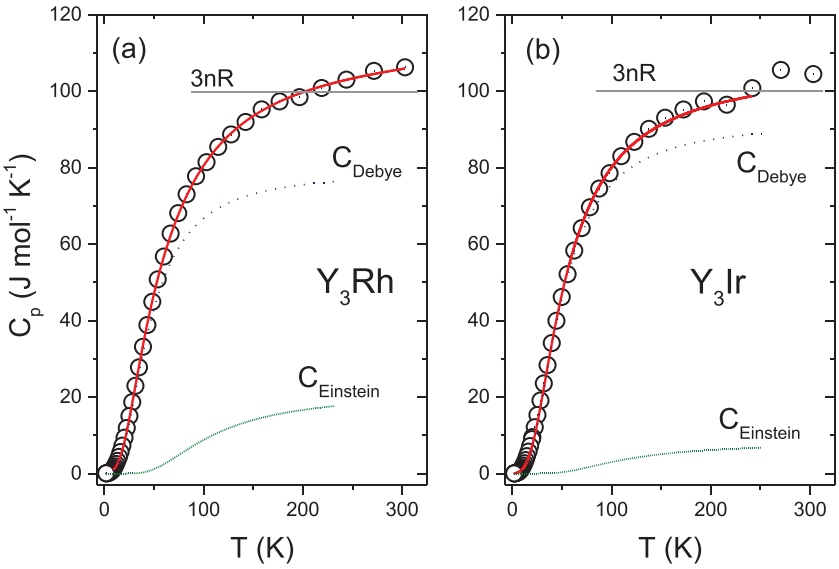

Figure 8. The black, empty circles present heat capacity C_p of (a) Y_3Rh and (b) Y_3Ir versus temperature T, respectively. The temperature range was from 2 K to 300 K, measurements performed in zero magnetic field. The red solid curves are the fitted sum of the contributions from electronic heat capacity (γT), the Debye lattice heat capacity (C_{Debye}) and the Einstein lattice heat capacity (C_{Einstein}).

$$C_p = \gamma T + kC_{\mathrm{Debye}}(T) + (1-k)C_{\mathrm{Einstein}}(T), \tag{4}$$

where the k parameter corresponds to the weight of phonon contributions to the specific heat given by the Debye (C_{Debye}) and Einstein (C_{Einstein}) models, respectively. The Debye model is given by expression (3), whereas the Einstein model is given below:

$$C_{\mathrm{Einstein}}(T) = 3nR\left(\frac{\Theta_{\mathrm{E}}}{T}\right)^2 \exp\left(\frac{\Theta_{\mathrm{E}}}{T}\right)\left[\exp\left(\frac{\Theta_{\mathrm{E}}}{T}\right)-1\right]^{-2}. \tag{5}$$

In figure 8, the fits are represented by red solid lines, whereas C_{Debye} and C_{Einstein} are shown by dashed and solid lines, respectively. In the fitting procedure, the Debye temperatures were fixed with values taken from the low temperature fit.

The estimated Einstein temperature is between 199 K (Y_3Pt) and 337 K (Y_3Rh) with the largest weight $(1-k)$ of C_{Debye} to the specific heat observed for Y_3Ni (28%) and Y_3Rh (21%).

4. Theoretical studies

To illuminate the problem whether electronic interactions are present in studied materials, Density functional theory (DFT) electronic structure calculations were performed. Experimental crystal structures of the studied materials [9, 10, 14, 18, 28] were used in computations. Full potential linearized augmented plane wave (FP-LAPW) method, as implemented in the WIEN2k code [29], was used, with the Perdew–Burke–Ernzerhof generalized gradient approximation [30] (PBE-GGA) exchange-correlation potential. Computations were done on a dense k-point mesh of about 10 000 points in the Brillouin zone, and included spin–orbit (SO) coupling. Comparison with the scalar-relativistic computations showed, that spin–orbit coupling becomes important for heavier M elements, starting from Pd. The total densities of states (DOS) and atomic contributions from M, Y(4c) and Y(8d) atoms are presented in figure 9. The values of the DOS at the Fermi energy, $N(E_{\mathrm{F}})$, are given in table 3.

As far as the number of valence electrons is concerned, the studied series of compounds may be divided into two isoelectronic groups: one for M = Co, Rh, Ir, with 18 valence electrons per f.u. (72 per unit cell), and the other for M = Ni, Pd, Pt, with 19 valence electrons per f.u. (76 per unit cell). The general shape of the DOS of all materials is schematically similar: an almost filled d shell of the M element is located 1–3 eV below the Fermi level (E_{F}), and this is responsible for the zero magnetic moments, even for the case of M = Co and Ni. A similar DOS profile was earlier reported for La_3Co and La_3Ni in [6]. Our results also remain in agreement with DFT computations reported for Y_3Co in [18] and XPS studies reported for Y_3Ni in [31]. However, the details of the electronic structure differ among the materials, showing the impact of the increase in the M-elements' atomic number. In the first row of figure 9, for the lightest M = Co (figure 9(a)), the 3d DOS shell starts to develop about −1 eV below E_{F}. Substitution of Co with Ni pushes E_{F} towards higher energies, due to an increase in the electron count, and E_{F} is located on

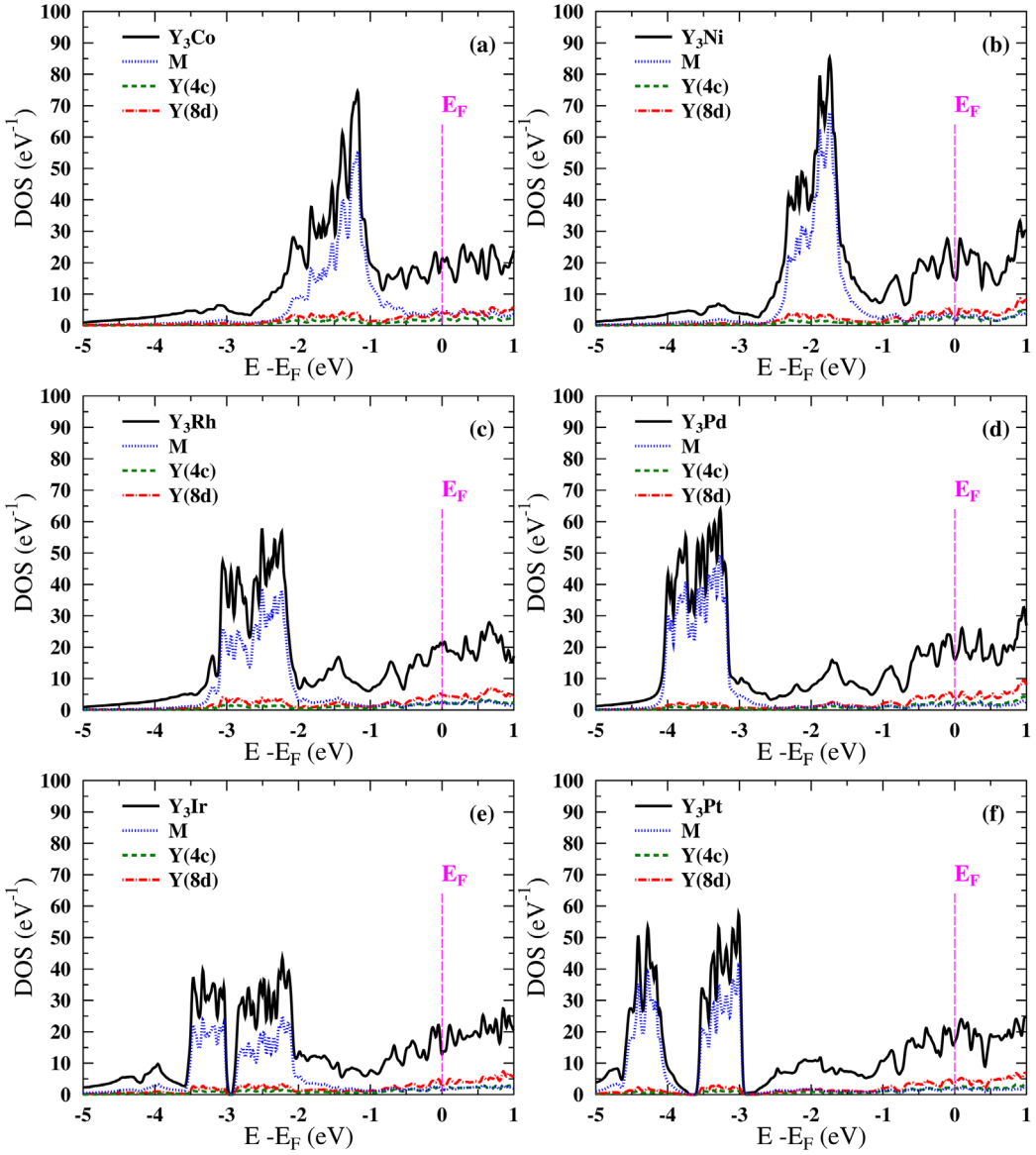

Figure 9. Computed densities of states for Y_3M compounds ((a) Y_3Co, (b) Y_3Ni, (c) Y_3Rh, (d) Y_3Pd, (e) Y_3Ir, (f) Y_3Pt), with spin–orbit coupling taken into account. DOS is given per unit cell of the crystal (4 formula units).

Table 3. Y_3M: values of density of states at the Fermi level $N(E_F)$ in eV^{-1} per formula unit. Atomic contributions are given in eV^{-1} per one atom. 'Bare' value of the Sommerfeld coefficient (mJ mol^{-1} K^{-2} per f.u.) is denoted as γ_0, experimental values γ are repeated after table 2 for convenience. Renormalization factor λ is calculated following equation $\gamma = \gamma_0(1 + \lambda)$.

$M =$	TDOS	M	Y(4*c*)	Y(8*d*)	γ_0	Γ	λ
Co	5.53	0.99	0.54	0.55	13.0	16.7	0.28
Ni	3.85	0.52	0.44	0.39	9.1	15.5	0.71
Rh	5.20	0.57	0.56	0.59	12.2	18.6	0.52
Pd	4.05	0.33	0.47	0.45	9.5	19.5	1.05
Ir	2.89	0.33	0.33	0.31	6.8	14.0	1.05
Pt	4.17	0.40	0.47	0.48	9.8	16.8	0.71

a slope in a local DOS minimum, seen a little above E_F for Y_3Co. This results in a smaller $N(E_F) = 3.8\,eV^{-1}$ per f.u., compared to $5.5\,eV^{-1}$ for the Co case (see, table 3). Again, this resembles the differences in electronic structures between superconducting La_3Co and La_3Ni [6]. For the 4*d* elements, $M =$ Rh and Pd, stronger bonding of the 4*d* shell pushes the characteristic DOS maximum another 1 eV deeper below E_F, and a broadening of the DOS peak is due to stronger spin–orbit coupling, which starts to separate the $d_{3/2}$ and $d_{5/2}$ electronic states. Also, here with the additional electron of Pd, compared to Rh, E_F is placed in a smaller DOS region. The heaviest case of $M =$ Ir and Rh, shows the strongest influence of the spin–orbit interaction on the DOS of the *M* element's d shell. Here, we

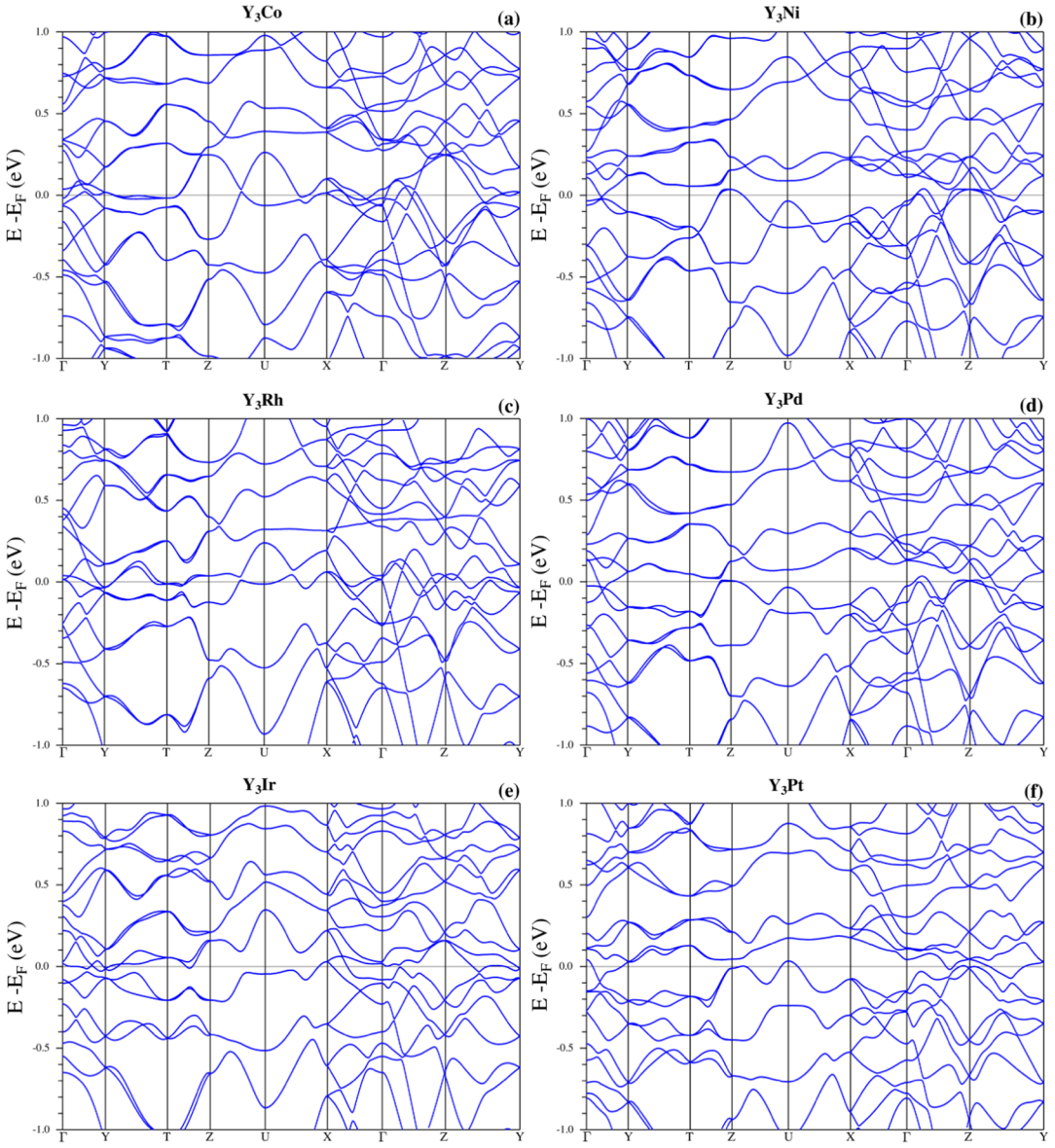

Figure 10. Electronic band structure of Y_3M compounds ((a) Y_3Co, (b) Y_3Ni, (c) Y_3Rh, (d) Y_3Pd, (e)Y_3Ir, (f) Y_3Pt) in the vicinity of the Fermi energy. For the location of high symmetry points in the Brillouin zone, see e.g. [6].

observe a clear splitting of the 5*d* shell and strongest bonding of 5*d* resulting electronic states, when compared to 4*d* and 3*d* orbitals of previous elements. Interestingly, here the tendency for a change in $N(E_F)$ in a row is opposite to previous cases. Due to additional changes in electronic band structure, the total DOS for Y_3Ir becomes smallest among the studied materials, as a local DOS valley is formed around the Fermi level (see, figure 9(e) and table 3).

Electronic dispersion relations in the vicinity of the Fermi energy are plotted in figure 10. Relatively large differences between all the materials are seen, which proves that the electronic structure near E_F is far from rigid, both due to the changes of the *M* elements' atomic number and small differences in crystal structures. Analysis of E(k) relations explain the above-mentioned differences in $N(E_F)$, while the *M* element is changed. First, analyzing in-a-period trends for 3*d* and 4*d* M elements (Co versus Ni and Rh versus Pd) we observe a formation of a large area in the Brillouin zone where E_F does not cross any band (Ni and Pd case, *Y*-*T* and *U*-*X*-Γ directions in figures 10(b) and (d)), which is caused both by the shift of E_F and modifications of the $E(k)$ shape. This results in lower DOS values for Y_3Ni and Y_3Pd, compared to Y_3Co and Y_3Rh. The fact that Y_3Co has the largest calculated $N(E_F)$ value is well reflected in a large number of relatively flat bands, crossing E_F in *X*-Γ-*Z* directions. This part of the $E(k)$ plot becomes less 'dense' for the $M =$ Rh case, and for $M =$ Ir only two bands are crossing E_F there.

Additionally, for Y_3Ir, modifications of the $E(k)$ shape reduce the number of bands crossing E_F in *Y*-*T*-*Z* directions, and the band centered at the *U* point hides below E_F, which results in the lowest $N(E_F)$ value among Y_3M compounds studied here.

Using the calculated total densities of states at the Fermi level, band structure values of the Sommerfeld coefficient are computed, as $\gamma_0 = \frac{\pi^2}{3} k_B^2 N(E_F)$, and compared to the experimental ones in table 3. Similarly to what was done for

a well-known example of a Fermi liquid system $TiBe_2$ [32], we may write $\gamma = \gamma_0(1 + \lambda_{ph})\frac{m^*}{m}$, where λ_{ph} is the electron–phonon coupling parameter. Now, taking $\frac{m^*}{m} = 1 + \lambda_e$, with λ_e describing the effective mass renormalization due to the electronic interactions, neglecting the smallest $\lambda_{ph}\lambda_e$ term one gets $\gamma = \gamma_0(1 + \lambda_{ph} + \lambda_e) \equiv \gamma_0(1 + \lambda)$. Values of λ, defined by this equation, are also shown in table 3, and comparison reveals noticeable renormalization of the electronic specific heat among Y_3M compounds, confirming the presence of interacting electrons. Renormalization factor λ varies from 0.28 (M = Co) to 1.05 (M = Ir, Pd). The situation found here is similar to what was found for sister compounds La_3Co and La_3Ni in [6], where $\lambda = 1.59$ (Co) and $\lambda = 0.73$ (Ni) were reported. In those materials, a large part of the enhancement factor λ came from the electron–phonon interaction, which was attainable for quantitative analysis due to their superconductivity. However, the observed superconducting critical temperatures were too low to ascribe the whole enhancement of γ to the electron–phonon coupling via λ_{ph}, and moderate collective electronic interactions of the form of spin fluctuations, competing with superconductivity, were suggested as the additional source of effective mass enhancement [6]. For Y_3M compounds a similar scenario may be possible, with part of the λ coming from electron–phonon interactions, and the rest from the electron–electron or even electron-paramagnon (spin-fluctuations) interactions, as suggested before [7] for Y_3Ni. If the electron–electron interactions take form of the spin fluctuations, a logarithmic term in specific heat C_p may be observed [32] $C_p/T = \gamma + \beta T^2 + \delta T^2 \ln T$. For our case, the fitting with the additional $\delta T^2 \ln T$ term (not shown here) does not improve the fit, thus we are not able to unambiguously conclude on the presence or absence of spin fluctuations contributing to the specific heat.

Comparing to La_3Co and La_3Ni materials, as no superconductivity was found in our studies down to 1.9 K in Y_3M, either weaker electron–phonon coupling or stronger electronic interactions should be present. Taking the literature data, small amounts of a superconducting phase was found in Y_3Co with $T_{c\,onset} = 0.34$ K, whereas superconductivity, with $T_c = 0.65$ K, was confirmed only for Y_3Rh [33]. Having this limited information on superconductivity in the Y_3M series, and especially no information whether the remaining compounds do not superconduct, or just have $T_c < 1.9$ K, a reliable decoupling of λ to the phonon contribution λ_{ph} and electronic contribution λ_e is possible only for Y_3Rh, and assuming electronic interactions take the form of spin fluctuations. Using the same procedure as applied for La_3Co in [6] we take $\lambda = \lambda_{ph} + \lambda_{sf}$. Next, we can use the experimental superconducting critical temperature of Y_3Rh, $T_c = 0.65$ K, Debye temperature $\Theta_D = 186$ K, McMillan's T_c formula [34]:

$$T_c = \frac{\Theta_D}{1.45} \exp\left[\frac{-1.04(1 + \lambda_{eff})}{\lambda_{eff} - \mu^*_{eff}(1 + 0.62\lambda_{eff})}\right]$$

where for the spin-fluctuations case the effective coupling parameter $\lambda_{eff} = \frac{\lambda_{ph}}{1 + \lambda_{sf}}$ and the enhanced Coulomb repulsion constant $\mu^*_{eff} = \frac{\mu^* + \lambda_{sf}}{1 + \lambda_{sf}}$ should be taken [35, 36]. Comparison of the measured and calculated Sommerfeld coefficient for Y_3Rh gave $\lambda = 0.52$ (see, table 3). Assuming a typical 'bare' value of the Coulomb pseudopotential parameter $\mu^* = 0.13$ we arrive at $\lambda_{ph} = 0.497$ and a small $\lambda_{sf} = 0.023$, which reproduce experimental $T_c = 0.65$ K. For Y_3Co, the renormalization factor λ is too small even to reproduce $T_c = 0.34$ K without the presence of any additional electronic interactions, thus the small amounts of superconducting phase, detected in [33] in the Y_3Co sample, might have been of another chemical composition. For the remaining compounds, putting 1.9 K as the upper limit for the possible superconducting transition temperature, we may roughly estimate lower limits of $\lambda_{sf} \approx 0.05$ for M = Ni, Pt, and larger $\lambda_{sf} \approx 0.15$ for M = Pd and Ir, close to values proposed in La_3Ni (0.05) and La_3Co (0.17) [4]. A similar magnitude of $\lambda_{sf} \approx 0.10$ was also postulated for the related system Y_4Co_3 [28], which is a magnetic superconductor, and where $\rho \propto T^2$ and $\rho \propto T^{5/3}$ resistivity behavior due to spin fluctuations were experimentally observed [29].

5. Conclusions

In conclusion, Y_3M compounds (M = Co, Ni, Rh, Pd, Ir, Pt) were synthesized and investigated with crystallographic, electrical resistivity, heat capacity measurements, and electronic band structure calculations. In each case a desired material was obtained with traces of an impurity phase detected for Y_3Pd, Y_3Pt, and Y_3Rh. In the latter, the impurity phase was found to be the previously unreported compound Y_5Rh_2 crystalizing in a monoclinic Pd_5B_2-type structure. Resistivity measurements reveal a metallic-like behaviour for all tested compounds, with RRR ranging from 1.3 to 8.3. No signs of superconductivity were detected above 1.9 K. An inflection of the resistivity below 160 K, that is observed for Y_3Co, originates from a charge density wave formation [18]. A small feature in the heat capacity data is also seen at the same temperature. All compounds exhibit a power-law temperature dependence of resistivity, with $\rho \propto T^n$ and $1.6 \leqslant n \leqslant 2.2$, indicating a possible influence of electron–electron interactions on the transport properties of the materials.

The Debye temperature and Sommerfeld coefficient were derived from the fit to low temperature heat capacity data. The estimated Debye temperature ranges from 180 K (Y_3Pt) to 222 K (Y_3Co). The highest value of the

Sommerfeld coefficient was found for Y_3Pd (19.5 mJ mol^{-1} K^{-2}) and Y_3Rh (18.6 mJ mol^{-1} K^{-2}), for which compounds we got the largest value of RRR. The heat capacity data were fitted in the whole temperature range by using the formula that includes the electronic part and the lattice part given by the Debye and Einstein model. It was found that the high energy optical modes (Einstein) are not required for the fit for Y_3Co. Comparing the calculated or measured phonon spectrum for Y_3Co and Y_3Ni or Y_3Rh, should shed light on this discrepancy.

The calculated Kadowaki–Woods ratios for Y_3Co and Y_3Ni are similar to those reported for the La-analogues (La_3Co and La_3Ni) and exceed the 'universal' value $10^{-7}\,\Omega\,m\,(J\,mol^{-1}\,K^{-1})^{-2}$ for heavy-fermion compounds.

Theoretical calculations show, that in general the electronic structures of Y_3M materials are similar, all having the mostly occupied *d* shell of the *M* atom a few eV below the Fermi level. However, a closer look at computed densities of states and electronic dispersion relations reveal an evolution of the electronic structure with the change of the *M* atom and an increasing importance on spin–orbit coupling. A comparison of the theoretical and experimental values of the Sommerfeld coefficient show enhancement of γ, and the renormalization parameter increases from 0.28 (Y_3Co) to 1.05 (Y_3Ir and Y_3Pd). In line with the almost quadratic temperature behavior of resistivity, the suggested possible source of renormalization are electron–phonon and electron–electron interactions, similar to La_3Co and La_3Ni compounds, where the presence of spin fluctuations was suggested.

While La_3Ni is a superconductor ($T_c \sim 1.45$ K [27]), no superconductivity was found in Y_3Ni. For Y_3Co a CDW formation is observed, whereas La_3Co is a superconductor with possible spin fluctuations. Since superconductivity with $T_c = 0.65$ K was reported for Y_3Rh [33], studying the suppression of the CDW, and enhancement of superconductivity, in a solid solution $Y_3Co_{1-x}Rh_x$ may therefore be of great interest.

Acknowledgments

This project was financially supported by the National Science Centre (Poland) Grant No. DEC-2012/07/E/ST3/00584. BW was partially supported by the Polish Ministry of Science and Higher Education. The authors would like to thank Elizabeth Carnicom (Princeton University) for improving the use of English in the manuscript.

References

[1] Dshemuchadse J and Steurer W 2015 Some statistics on intermetallic compounds *Inorg. Chem.* **54** 1120–8
[2] Momma K and Izumi F 2011 VESTA 3 for three-dimensional visualization of crystal, volumetric and morphology data *J. Appl. Crystallogr.* **44** 1272–6
[3] Baranov N V, Andreev A V, Kozlov A I, Kvashnin G M, Nakotte H, Aruga Katori H and Goto T 1993 Magnetic phase transitions in Gd_3Co *J. Alloys Compd.* **202** 215–24
[4] Baranov N V, Yermakov A A, Markin P E, Possokhov U M, Michor H, Weingartner B, Hilscher G and Kotur B 2001 Magnetic phase transitions, short-range correlations and spin fluctuations in $(Gd_{1-x}Y_x)_3Co$ *J. Alloys Compd.* **329** 22–30
[5] Fisk Z and Lawson A C 1973 Normal state resistance behavior and superconductivity *Solid State Commun.* **13** 277–9
[6] Strychalska J, Roman M, Sobczak Z, Wiendlocha B, Winiarski M J, Ronning F and Klimczuk T 2016 Physical properties and electronic structure of La_3Co and La_3Ni intermetallic superconductors *Physica* C **528** 73–83
[7] Gratz E, Hilscher G, Michor H, Markosyan A, Talik E, Czjzek G and Mexner W 1996 Low temperature properties of Y_3Ni, Czechoslov *J. Phys.* **46** 2031–2
[8] Talik E, Neumann M, Slebarski A and Winiarski A 1995 Properties of Y_3Rh and Y_3Ir *Physica* B **212** 25–32
[9] Sanjines-Zeballos R, Chabot B and Parthé E 1980 Rare earth-osmium compounds R_3Os and Y_3Ru, Y_3Os and Y_3Pd with the Fe_3C structure *J. Common Met.* **72** P17–20
[10] Le Roy J, Moreau J M, Paccard D and Parthé E 1979 Rare-earth (and yttrium)–iridium and –platinum compounds with the Fe_3C structure type *Acta Crystallogr.* B **35** 1437–9
[11] Rodríguez-Carvajal J 1993 Recent advances in magnetic structure determination by neutron powder diffraction *Physica* B **192** 55–69
[12] Talik E, Szade J, Heimann J, Winiarska A, Winiarski A and Chelkowski A 1988 X-ray examination, electrical and magnetic properties of R_3Co single crystals (R ≡ Y, Gd, Dy and Ho) *J. Common Met.* **138** 129–36
[13] Subramanian P R and Smith J F 1985 Thermodynamics of formation of Y–Ni alloys *Metall. Trans.* B **16** 577–84
[14] Raman A 1972 Crystal structures of some Ln_3Rh, Ln_7Rh_3 and $LnRh_3$ phases *J. Common Met.* **26** 199–206
[15] Fornasini M L and Palenzona A 1974 Crystal structure of the so-called R.E.$_5Pd_2$ compounds *J. Common Met.* **38** 77–82
[16] Le Roy J, Paccard D and Moreau J-M 1980 R_5Ir_2 compounds (R = Pr, Nd, Sm, Gd, Tb, Dy, Ho, Er, Tm, Lu, Y) with the monoclinic Mn_5C_2 structure *J. Common Met.* **72** P11–5
[17] Palenzona A and Ciraflci S 1998 The Eu–Rh (europium–rhodium) system *J. Phase Equilibria* **19** 162
[18] Podlesnyak A, Ehlers G, Cao H, Matsuda M, Frontzek M, Zaharko O, Kazantsev V A, Gubkin A F and Baranov N V 2013 Temperature-driven phase transformation in Y_3Co: neutron scattering and first-principles studies *Phys. Rev.* B **88** 024117
[19] Bochenek L, Rogacki K, Kolodziejczyk A and Cichorek T 2015 *d*-band metal Y_9Co_7 revisited: evidence for local coexistence of superconductivity and itinerant ferromagnetism *Phys. Rev.* B **91** 235314
[20] Klimczuk T *et al* 2012 Superconductivity in the Heusler family of intermetallics *Phys. Rev.* B **85** 174505
[21] Gratz E, Hilscher G, Michor H, Bauer E, Kottar A and Markosyan A 1997 Temperature-dependent properties of Y_3Ni *Physica* B **237–8** 476–7
[22] Kolodziejczyk A and Spalek J 1984 Spin fluctuations in a very weak itinerant ferromagnet: Y_4Co_3, *J. Phys. F: Met. Phys.* **14** 1277
[23] Baym G and Pethick C 2014 *Landau Fermi-Liquid Theory: Concepts and Applications* (New York: Wiley)
[24] Tristan N V, Nenkov K, Skokov K and Palewski T 2004 Specific heat and magnetic susceptibility of intermetallic compounds R_3Ni *Physica* B **344** 462–9
[25] Kuentzler R and Loebich O 1985 Electronic properties and stability of the ordered Pd–Y alloys *J. Common Met.* **106** 335–48

[26] Lu Q F, Umehara I, Adachi Y and Sato K 1997 Single crystal growth of R_3Co (R: La, Pr and Nd) and their characteristic transport properties *Mater. Trans. JIM* **38** 1–4
[27] Sato N, Koga N, Imamura K, Sakon T and Komatsubara T 1995 Unusual properties of a new superconductor La_3Ni *Physica* B **206** 565–7
[28] Talik E and Slebarski A 1994 Lattice parameters of R_4Ni compounds (R = Y, Gd, Tb) *J. Alloys Compd.* **215** 213–6
[29] Blaha P, Schwarz K, Madsen G K H, Kvasnicka D and Luitz J 2001 *WIEN2K, an Augmented Plane Wave + Local Orbitals Program for Calculating Crystal Properties* ed K Schwarz (Tech. Univ. Wien) (http://susi.theochem.tuwien.ac.at/reg_user/textbooks/usersguide.pdf)
[30] Perdew J P, Burke K and Ernzerhof M 1996 Generalized gradient approximation made simple *Phys. Rev. Lett.* **77** 3865–8
[31] Talik E and Neumann M 1994 XPS investigations of Y_3Ni and Gd_3Ni single crystals *Physica* B **193** 207–12
[32] Stewart G R, Smith J L, Giorgi A L and Fisk Z 1982 Specific heat of well-characterized $TiBe_2$ at 0 and 7 T *Phys. Rev.* B **25** 5907–17
[33] Geballe T H, Matthias B T, Compton V B, Corenzwit E, Hull G W and Longinotti L D 1965 Superconductivity in binary alloy systems of the rare earths and of thorium with Pt-group metals *Phys. Rev.* **137** A119–27
[34] McMillan W L 1968 Transition temperature of strong-coupled superconductors *Phys. Rev.* **167** 331–44
[35] Wiendlocha B, Tobola J, Sternik M, Kaprzyk S, Parlinski K and Oles A M 2008 Superconductivity of Mo_3Sb_7 from first principles *Phys. Rev.* B **78** 060507
[36] Wiendlocha B, Tobola J, Kaprzyk S and Kolodziejczyk A 2011 Electronic structure, magnetism, and spin fluctuations in the superconducting weak ferromagnet Y_4Co_3 *Phys. Rev.* B **83** 094408